Translational Oncology
www.transonc.com

Volume 3 Number 6 December 2010 pp. 362–372 362

Human Lymphatic Architecture and Dynamic Transport Imaged Using Near-infrared Fluorescence[1,2]

John C. Rasmussen*,[3], I-Chih Tan*,[3], Milton V. Marshall*,[3], Kristen E. Adams*,[3], Sunkuk Kwon*,[3], Caroline E. Fife†,‡, Erik A. Maus†,‡, Latisha A. Smith†,‡, Kyle R. Covington§ and Eva M. Sevick-Muraca*,[3]

*Center for Molecular Imaging, The Brown Foundation Institute of Molecular Medicine at the University of Texas Health Science Center at Houston, Houston, TX, USA; †Department of Internal Medicine, Division of Cardiology and Hyperbaric Medicine at The University of Texas Health Science Center at Houston, Houston, TX, USA; ‡Memorial Hermann Hospital, Center for Lymphedema Management, Houston, TX, USA; §Translational Biology and Molecular Medicine, Baylor College of Medicine, Houston, TX, USA

Abstract

BACKGROUND: Although the importance of lymphatic function is well recognized, the lack of real-time imaging modalities limits our understanding of its role in many diseases. In a phase 0 exploratory study, we used dynamic, near-infrared (NIR) fluorescence imaging to assess the extremes of lymphatic architecture and transport in healthy human subjects and in subjects clinically diagnosed with unilateral lymphedema (LE), a disease that can be prevalent in cancer survivors. *METHODS AND RESULTS:* Active lymphatic propulsion was imaged after intradermal injections of 25 μg of indocyanine green (total maximum dose $\leq$400 μg) bilaterally in the arms or legs of control and subjects. Images show well-defined lymphatic structures with propulsive dye transport in limbs of healthy subjects. In LE subjects, we observed extravascular dye accumulation, networks of fluorescent lymphatic capillaries, and/or tortuous lymphatic vessels in all symptomatic and some asymptomatic limbs. Statistical models indicate that disease status and/or limb significantly affect parameters of apparent lymph propagation velocity and contractile frequency. *CONCLUSIONS:* These clinical research studies demonstrate the potential of NIR fluorescence imaging as a diagnostic measure of functional lymphatics and as a new tool in translational research studies to decipher the role of the lymphatic system in cancer and other diseases.

Translational Oncology (2010) 3, 362–372

Introduction

The lymphatic system is composed of a network of capillaries, vessels, trunks, ducts, and lymph nodes that collect fluid, macromolecules, proteins, and immune cells from the interstitial space, transport the fluid or lymph, and return it to the venous system [1]. Unlike the hemovascular system, the lymphatics do not have a centralized pumping organ, and lymph is transported through the lymphatics, primarily by cyclic contractions of vessel subunits called lymphangions. Bounded by valves to ensure unidirectional flow, lymphangions are arranged in series and sequentially contract to propel the lymph through the lymphatics in a peristaltic manner [1]. Although contractile function is crucial to the

Address all correspondence to: Eva M. Sevick-Muraca, Center for Molecular Imaging, The Brown Foundation of Molecular Medicine, The University of Texas Health Science Center, SRB 330A, Houston, TX 77030. E-mail: eva.sevick@uth.tmc.edu

[1]This work was supported in part by the Longaberger Foundation through an American Cancer Society Research Scholar Grant (RSG-06-213-01-LR) and the National Institutes of Health (R01 HL092923 and U54 CA136404) to E.M.S. The authors have no competing financial interests.

[2]This article refers to supplementary materials, which are designated by Tables W1 to W4, Figures W1 and W2, and Videos W1 to W4, and are available online at www.transonc.com.

[3]Formerly of the Department of Radiology, Baylor College of Medicine, Houston, TX. Portions of this work were conducted at Baylor College of Medicine.

Received 8 July 2010; Revised 26 August 2010; Accepted 30 August 2010

 1944-7124/10/$25.00
DOI 10.1593/tlo.10190

transport of lymph, the fundamental physiological mechanisms governing this phenomenon are not well understood, and there are no methods to evaluate contractile function noninvasively in humans.

Disruption of lymph transport, because of impaired lymphatic function, reduced numbers of lymphatic vessels, valvular insufficiencies, or exacerbated by combinations of the above results in the chronic condition of lymphedema (LE) and its sequelae of inflammatory response results [2–4]. Treatment for LE is generally limited to compression bandaging and manual lymphatic drainage or massage to minimize swelling and encourage lymph drainage. There is no cure for lymphedema.

In Western countries, acquired LE is generally caused by trauma or surgery, typically after lymph node resection for cancer staging or therapy. It is estimated that, depending on the therapeutic approach taken, as many as 40% of all breast cancer patients who undergo axillary lymph node dissection [5–7] and 64% of all cancer patients who undergo groin lymph node dissection [8] encounter acquired LE. LE may present weeks to years after trauma or surgery, often after a challenge to the immune system. Although there are no means to predict who will develop "secondary" LE and when, recent work suggests that causal or susceptibility genes may be involved [9]. In contrast, hereditary or primary LE has been associated, thus far, with mutations in vascular endothelial growth factor receptor 3 [10,11] (Milroy or Miege disease), SOX18 [11], and FOXC2 [12–15] (lymphedema-distichiasis), in which the latter disease is noted for valvular insufficiencies and has been characterized by lymphoscintigraphy as exhibiting lymph reflux in dilated lymphatic vessels of the leg [13].

Currently, lymphoscintigraphy is the only means available to routinely image the lymphatics. Although gross lymph architecture such as main vessels and nodes are visualized in scintigrams, the long integration times associated with gamma cameras prevent imaging of real-time lymphatic contractile function and the spatial resolution limits visualization of fine lymphatic vasculature. Because the lymphatics provide little endogenous contrast, direct imaging of the lymphatics is difficult and lymphatic architecture and function generally cannot be probed directly with ultrasound, magnetic resonance, or computed tomography. In addition, the lymphatic vasculature is not readily accessible for administration of the milliliters of contrast agent needed for magnetic resonance or computed tomography angiography, making aberrant lymph architecture difficult to routinely assess (for reviews on lymphatic imaging, see Sharma et al. [16], Szuba and Rockson [17], and Lucarelli et al. [18]). In an extensive review, Marshall et al. [19] summarized the work of several groups who have developed optical imaging devices for human lymphatic imaging using near-infrared (NIR) fluorescence. In these studies, indocyanine green (ICG), a green dye used for hepatic clearance and ophthalmological indications, was used primarily to map the lymphatics and provide surgical guidance for nodal resection. Although these optical imaging devices are sensitive enough to image the lymphatics with milligram amounts of ICG, none have quantified contractile lymphatic function [19–23]. Recently, we demonstrated the feasibility for noninvasive imaging and quantification of propulsive, contractile lymphatic function after intradermal administration of *microgram* amounts of ICG [20,24].

The objective of the phase 0 clinical feasibility study described was to evaluate the utility of NIR fluorescence to 1) image differences within the lymphatic architecture and its contractile function and 2) quantify the apparent propagation velocity and frequency or period of contractile transport in the arms or legs of healthy control subjects as well as of subjects clinically diagnosed with unilateral LE. The ability to noninvasively visualize lymphatic architecture and quantify its propulsive function within asymptomatic and symptomatic limbs of subjects with LE as well as within the limbs of healthy subjects provides the first opportunity to investigate changes in lymphatic function with human disease.

Materials and Methods

Study Design

The protocol used for this feasibility study was approved by the US Food and Drug Administration under combinational exploratory investigational new drug application 76,920 for the off-label use of ICG as a NIR fluorescent contrast agent. The Health Insurance Portability and Accountability Act (HIPAA)-compliant studies were approved by the institutional review board at Baylor College of Medicine in Houston, Texas, where the study was conducted and by the institutional review board at the University of Texas Health Science Center at Houston, where the imaging data were evaluated. A total of 24 healthy volunteers and 20 subjects diagnosed with stage 1 or 2 unilateral LE were recruited for this study. The summarized demographic data for all 44 subjects imaged are presented in Table 1. The demographics, dosage, and disease cause for each subject are available in Tables W1, W2, W3, and W4. Persons weighing more than 400 lb (weight limit of bed) or with known sensitivity to iodine were excluded from the study as were minors and pregnant or nursing women. Half of the LE subjects had been clinically diagnosed with unilateral leg LE and half with unilateral arm LE. In this phase 0 study, we did not control for cause of LE, that is, whether acquired or primary; however, 3 of 10 leg LE subjects and 10 of 10 arm LE subjects were cancer survivors. Half of the healthy volunteers and LE subjects received intradermal injections of ICG in both arms and the remainder in both legs. Immediately after injection, all subjects were imaged with a custom-built NIR fluorescence imaging system [24]. Total imaging time varied from subject to subject, but was typically 2 hours. Subjects were supine during imaging, and vital signs were monitored for 2 hours after injections with follow-up calls made 24 and 48 hours later. No adverse events were associated with the drug or device in this feasibility study. Neither the effects of demographics (e.g., sex, age, weight, and ethnicity) nor physiological

Table 1. Demographic Characteristics of Subjects Imaged.

Characteristic	Healthy (n = 24)	Lymphedema (n = 20)	
Sex, n (%)			
Male	5 (20.8)	1 (5.0)	
Female	19 (79.2)	19 (95.0)	
Age, mean ± SD,* years	38.2 ± 11.0	49.7 ± 17.6	
Mean weight, kg ± SD*	72.7 ± 12.1	74.3 ± 21.3	
Body surface area,† m^2 ± SD*	1.8 ± 0.2	1.8 ± 0.2	
Ethnicity, n (%)			
Caucasian	19 (79.2)	15 (75.0)	
Black	2 (8.3)	3 (15.0)	
Asian	2 (8.3)	1 (5.0)	
Hispanic	1 (4.2)	1 (5.0)	
Other	0 (0.0)	0 (0.0)	
Limb, n (%)			
Leg	12 (50.0)	10 (50.0)	
Arm	12 (50.0)	10 (50.0)	
Cause of disease, n (%)		Arms (n = 10)	Legs (n = 10)
Primary	—	0 (0.0)	3 (30.0)
After cancer treatment	—	10 (100.0)	3 (30.0)
After injury	—	0 (0.0)	2 (20.0)
Insect bite	—	0 (0.0)	2 (20.0)

*SD indicates standard deviation.

†Body surface area calculated by the DuBois formula.

factors contributing to lymphatic transport (e.g., pressure, stress) were considered in this limited feasibility study.

Injection of Contrast Agent

ICG is a tricarbocyanine dye that is approved for hepatic, cardiovascular, and ophthalmology applications. It is typically administered systemically in adults with the total dose not exceeding 2 mg/kg. On administration, ICG associates to albumin and is subsequently taken up by the liver and secreted into the bile. With a biologic half-life of 2 to 4 minutes in the blood, ICG has been used safely for more than 50 years [25]. The dye can be excited between 760 and 785 nm, and the emitted fluorescent signal can be collected between 820 and 840 nm. ICG exhibits a subnanosecond fluorescent lifetime, indicating the lack of the existence of a triplet state and formation of damaging free radicals on excitation.

For these studies, ICG was reconstituted in water to a base concentration of 2.5 mg/ml and subsequently diluted with saline to achieve a final concentration of 0.25 mg/ml. Each subject received up to 16 intradermal injections of 0.1 ml of diluted ICG for a maximum total dose of 400 μg. Injection sites varied owing to areas of fibrosis in LE subjects. In the arms, four injections were administered between the digits of each hand for a total dose of 200 μg of ICG, or when fibrosis made interdigital injection difficult, a total of six injections were made on each arm, typically with two on the top of the hand, two on the medial forearm, and two on the lateral forearm for a total dose of 300 μg of ICG. Generally, eight injections were administered on each leg (two on top of the foot, two on the medial ankle, one on the heel, two on the calf, and one on the thigh) for a total dose of 400 μg of ICG. One LE leg subject declined additional injections after two injections were administered for a total dose of 50 μg. In all cases, the injection sites for individual subjects matched between right and left limbs. Ten subjects requested use of a topical anesthetic with lidocaine 2.5% and prilocaine 2.5% cream applied directly to the injection site to lessen the injection sensation. For this study, the clinically identified diseased limbs of unilateral LE subjects are referred to as symptomatic, the clinically unaffected limbs are referred to as asymptomatic, and all limbs of the controls subjects are referred to as normal or control.

NIR Fluorescence Imaging

After intradermal injection, the injection sites were covered with black vinyl tape to prevent camera oversaturation. The location and movement of the ICG in each limb was then imaged simultaneously using two custom-built fluorescence imaging systems (see Video W1 for transit of ICG immediately after administration). During the imaging session, each imaging system was used to scan the lymphatics from the injection sites near the digits to the draining nodal basin to visualize the lymphatics of the entire limb. Occasionally, bilateral limbs were imaged with a single imaging system. Each system consists of a 785-nm excitation light source, an NIR-sensitive image intensifier, and a customized charge-coupled device (CCD) camera outfitted with filters to collect fluorescence at 830 nm. After imaging the first eight control subjects, the original 80-mW laser diode used to provide the 785-nm excitation light source was replaced with a 500-mW laser diode to provide a broader, brighter, and more uniform illumination of the field of view, resulting in sharper and more detailed fluorescent images. The emitted excitation light was attenuated using an optical diffuser such that a maximal tissue surface area of approximately 900 cm^2 was illuminated with less than 1.9 mW/cm^2. Excitation light propagated through tissues to activate the injected ICG. The generated fluorescent signal that emanated from the tissues was filtered with a 785-nm holographic notch filter (optical density ≥6) and an 830-nm band-pass filter (optical density ≥4). A 28-mm Nikkor lens (Nikon, Melville, NY) was used to focus the fluorescent signal onto the photocathode of a Gen 3 image intensifier. The intensified image was acquired with a customized, 16-bit, frame transfer, CCD camera. An exposure time of 200 milliseconds and a total acquisition time of ~650 milliseconds per image permitted near real-time imaging of the lymphatics *in vivo* and enabled compilation of images to create movies. All supplemental videos (available online) are approximately three times faster than real time.

Quantification of Lymphatic Function

The two-dimensional fluorescent images were previewed using ImageJ (National Institutes of Health, Bethesda, MD) to visually identify subsets of images containing lymphatic contractile function as distinguished by the movement of "packets" of higher fluorescent intensity along the lymphatic vessels from the regions of high dye concentration near the injection sites to the regional nodal basin. A custom MATLAB (MathWorks, Natick, MA) program was then used to identify regions of interest (ROIs) along the length of the lymphatic vessels and to calculate the apparent distance each fluorescent packet traveled between ROIs. The distance is denoted as apparent to reflect the lack of information in the third dimension. Apparent propagation velocity was computed by dividing the apparent distance traveled by the travel time of the fluorescent packet. In cases where fluorescence was observed to move distally from the local draining lymphatic basin, the apparent velocities were reported as negative. The period was measured as the time lapse between consecutive lymphatic propulsion events in the same ROI. In this initial feasibility study, limbs were interrogated by scanning the camera field of view across the entire limb. Because we did not always observe consecutive pulsatile events, there are fewer period measurements than velocity measurements. To account for the variable imaging time and the variable number of propulsion events observed in each limb, we computed the overall propulsion rate for each subject by dividing the total number of observed packets in each limb by the total time spent imaging that limb. Total imaging time is the time difference between when the first image was taken and when the last image was obtained.

Because ICG concentration, lymphatic vessel diameter and depth, and skin pigmentation may not be expected to be constant across the length of a lymphatic vessel, the re-emitted fluorescence may be expected to vary across the length of the vessel. As ICG-laden lymph is propelled toward the draining lymph node basins, it is diluted by non ICG-laden lymph collected from the initial collecting lymphatics located away from the injection site. As lymphangions fill and empty of ICG-laden lymph, their fluorescent intensity will also increase and decrease with time. Because we measure the time rate of change of fluorescence intensity at a single location to denote a "pulse," spatial variations across the length of a vessel do not affect our quantitative values of apparent velocity, period, or propulsion rate. All images presented herein are in pseudocolor.

Statistical Analysis

Whereas this was a feasibility trial and therefore not powered for statistics, we performed some statistical analyses to determine which variables may affect the quantified data. *R: A Language and Environment for Statistical Computing* [26] was used to model the effects of limb (arm or leg), diagnosis (control, symptomatic, or asymptomatic), side (right or left), dose of ICG, and topical anesthesia (with or without) for all

values of apparent velocity and period as well as the effect of diagnosis, limb, side, and dose on the overall propulsion rate. The lme4 package in R was used to create linear models for these data, which included the overall and the within subject effects of the factors. The factors were considered significant if their inclusion in the model resulted in a significantly better ($P < .05$) model fit than a model excluding them. Because of the distributions of these data and the presence of negative values in the raw data, period and apparent velocity measures were converted to ranks for modeling.

Results

Table 2 summarizes the quantified data by diagnosis and limb, including the number of apparent propagation velocity and period measurements, their ranges, medians, means and SDs, as well as the overall propulsion rates. Tables W1, W2, W3, and W4 summarize 1) the apparent velocities as determined from the movement of fluorescent packets within the vessels because of lymphatic contractions, 2) the period between consecutive contractile events, 3) the overall propulsion rates, and 4) pertinent comments for individual control and LE subjects. For pooled measurements ($n = 3423$ for apparent velocity and $n = 1738$ for period) of all 44 subjects in the study, our linear models indicate that diagnosis (i.e., control, asymptomatic, or symptomatic) has a significant effect on both the apparent propagation velocity ($P < .0005$) and period ($P < .005$) and that limb (i.e., arm or leg) has a significant effect on the period ($P < .01$) but not apparent velocity. The models indicate no significant effect on the apparent propagation velocity or period due to side (i.e., left or right), dose, or the application of local, topical anesthetic. The data from 10 subjects who received topical anesthetic comprised 739 of the total 3423 values of apparent velocity and 361 of the total 1738 values of period. Monte Carlo simulation, using the available data as a model, demonstrated sufficient power to detect a significant effect of the topical anesthetic on apparent propagation velocity or period had one existed, at a P value of less than 0.05 and a power greater than 80%. In the following, we focus on lymphatic architecture and the quantification of lymphatic transport due to contractile function in control limbs as well as in the limbs of subjects with clinically diagnosed unilateral LE. Specific cases presented below reference subject identification codes found in Tables W1, W2, W3, and W4.

Control Arms

Although the number and anatomic map of lymphatic vessels varied between control subjects, the lymphatic structure generally consisted of well-defined channels as illustrated in Figure 1. Figure 1*A* shows the web of lymphatic vessels in the dorsal left hand after four interdigital injections of ICG; Figure 1*B* shows the lymphatic vasculature in the medial right elbow; and Figure 1, *C* and *D*, shows the lymph vessels in the upper and entire right arm, respectively. Active contractile function with propagation toward the axilla, as shown in Video W2, was observed in all control arms. However, contractile function was not observed in every fluorescent vessel. Axillary and cubital lymph nodes were observed in some subjects.

Figure 2 illustrates the fluorescent intensity profiles as a function of time for two ROIs along a lymphatic vessel in the medial arm (Figure 2*A*). As the packet propagates through each ROI, a peak in fluorescent intensity is observed. Figure 2*B* shows that ROI 1 (blue) fills and empties its contents into ROI 2 (red). The apparent propagation velocity is calculated by dividing the apparent distance between ROIs 1 and 2 by time difference between the corresponding intensity peaks, whereas the period is defined by the time lapse between successive intensity peaks in the same ROI. The mean ± SD apparent propagation velocity and period measured in the control arms was 0.8 ± 0.4 cm/sec and 48.2 ± 36.8 seconds, respectively, as shown in Table 2. The mean ± SD propulsion rate, defined by the total number of propulsion events (i.e., velocity measurements) divided by the total time imaged, is 1.3 ± 1.2 propulsions per minute, as also shown in Table 2.

Control Legs

Similar to that of arms, the lymphatic architecture in the legs also varied between control subjects, but generally consisted of well-defined structures as illustrated in Figure 3. Figure 3*A* illustrates the web of lymphatics in the dorsum of the left foot after two injections of ICG approximately one inch above the digits (see Video W3 for visualization of lymphatic flow in the foot). In Figure 3*B*, the lymphatics located in the medial right leg are shown; in Figure 3*C*, two lymphatic vessels are visible in the right patellar fossa; and in Figure 3*D*, deep lymphatics vessels draining toward the inguinal lymph node basin in the left leg are shown. Lymphatic vessels located deep within the leg appear diffuse owing to the scatter of light from intervening tissues. In five subjects (indicated in Tables W1 and W2), tortuous lymphatic vessels were also seen. In one control limb, a small area of extravascular dye was observed near an injection site, whereas several smaller vessels were observed radiating from an injection site another control limb. Lymphatic reflux or retrograde propagation of fluorescent packets toward the feet was observed in three control subjects. As shown in Table 2, the mean ± SD apparent propagation velocity in the legs was 0.9 ± 0.7 cm/sec, the mean ± SD period was 52.2 ± 36.1 seconds, and the overall propulsion rate was 0.4 ± 0.3 propulsions per minute. Inguinal and popliteal nodes were observed in some subjects.

Asymptomatic and Symptomatic Arms

The lymphatic architecture in LE subjects was markedly different than that in control subjects and was consistent with that seen by Unno

Table 2. Summary of Apparent Contractile Propagation Velocities and Periods.

Limb	No. Limbs	No. Velocity Measurements	Range (cm/sec)	Median (cm/sec)	Mean ± SD (cm/sec)	No. Period Measurements	Range (sec)	Median (sec)	Mean ± SD (sec)	Overall Propulsion Rate (Propulsions per Minute)
Control arm	24	1493	0.07 to 4.9	0.7	0.8 ± 0.4	803	2.3-250.5	34.6	48.2 ± 36.8	1.3 ± 1.2
Asymptomatic arm	10	731	−1.2 to 4.9	0.7	0.8 ± 0.4	402	2.8-200.0	29.9	39.7 ± 29.1	1.2 ± 1.0
Symptomatic arm	10	138	−4.2 to 4.1	0.7	0.7 ± 1.0	97	5.0-84.0	24.4	32.1 ± 17.9	0.3 ± 0.3
Control leg	24	734	−1.5 to 11.7	0.8	0.9 ± 0.7	273	3.2-193.8	43.2	52.2 ± 36.1	0.4 ± 0.3
Asymptomatic leg	10	194	0.1 to 2.7	0.7	0.8 ± 0.5	91	12.4-252.0	50.1	65.3 ± 46.4	0.3 ± 0.2
Symptomatic leg	10	133	0.1 to 1.9	0.7	0.8 ± 0.4	72	6.0-228.3	64.0	72.1 ± 45.1	0.2 ± 0.2

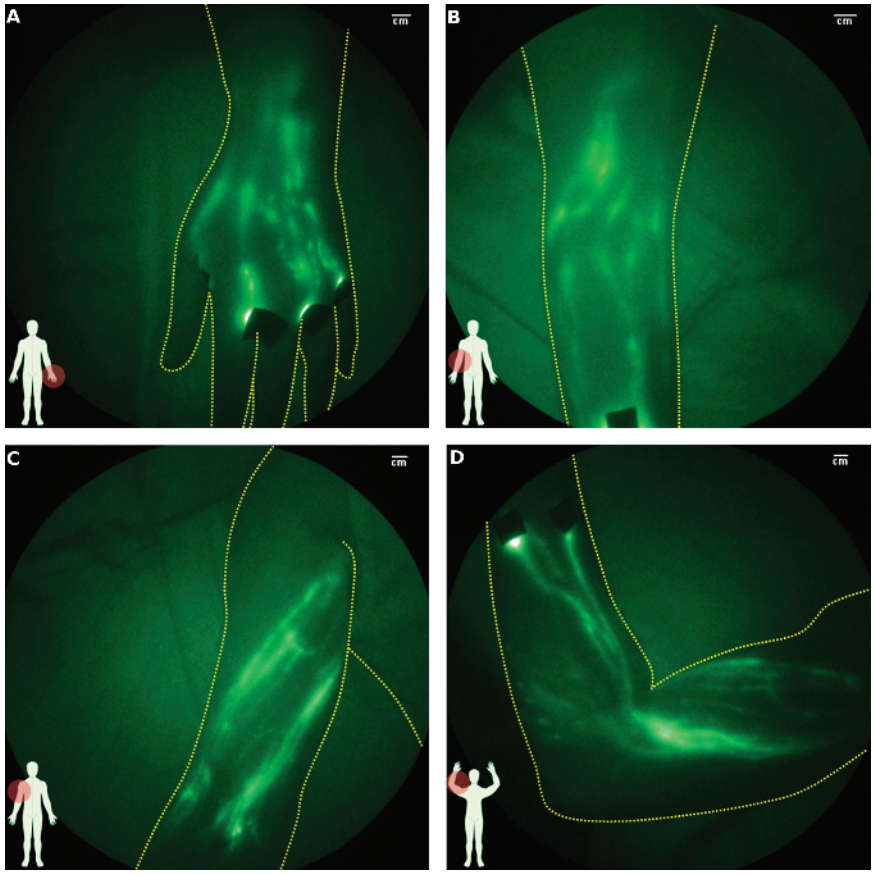

Figure 1. Images of lymphatics of control arm subjects: (A) left hand after interdigital injections (subject CA08), (B) right elbow (subject CA10, Video W1 shows typical lymphatic flow), (C) upper right arm (subject CA12), and (D) entire right arm from wrist to shoulder (subject CA12). Black spots are covered injection sites.

et al. [22]. Architectural abnormalities such as regions of diffused dye patterns arising from extravascular fluorescence and dense networks of capillary lymphatics were not typically observed in control subjects. Although tortuous vessels were observed in 5 of 48 control limbs, they were seen in nearly half of the 40 asymptomatic and symptomatic limbs (arms and legs).

Figure 4 illustrates symptomatic and asymptomatic hands and arms of typical subjects with acquired LE after breast cancer treatment. Figure 4*A*

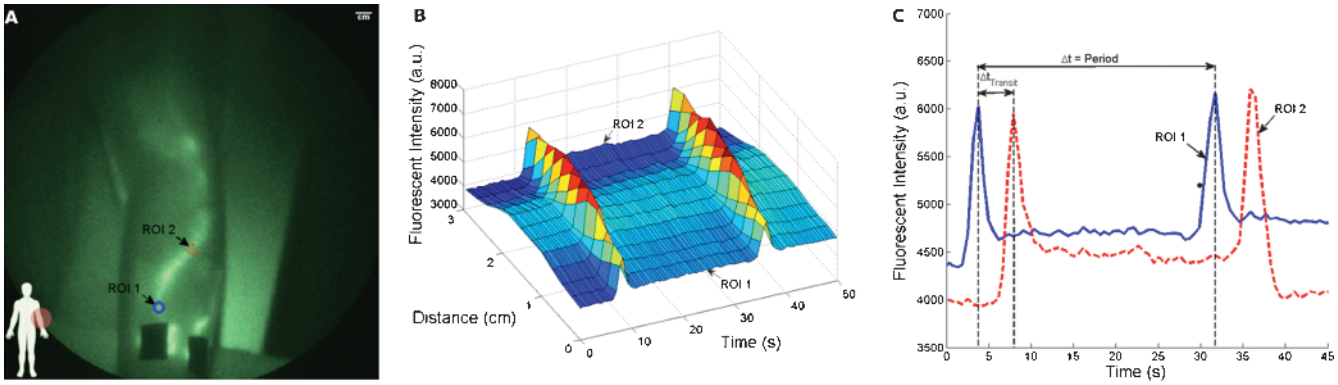

Figure 2. Quantitation of lymphatic function. Lymphatic function is quantified by analyzing the profiles of fluorescent intensity at two ROIs (A) on a medial arm of subject CA10. (B) The three-dimensional plot of fluorescent intensity as a function of time and distance illustrates the propagation of the fluorescent packet along the vessel. The distance traveled is defined as the distance between ROIs 1 and 2 in (A) and the transit time ($\Delta t_{Transit}$) is defined as the time lapse between corresponding intensity peaks in ROIs 1 and 2 as illustrated in (C). Period is the time lapse between successive peaks in the same ROI.

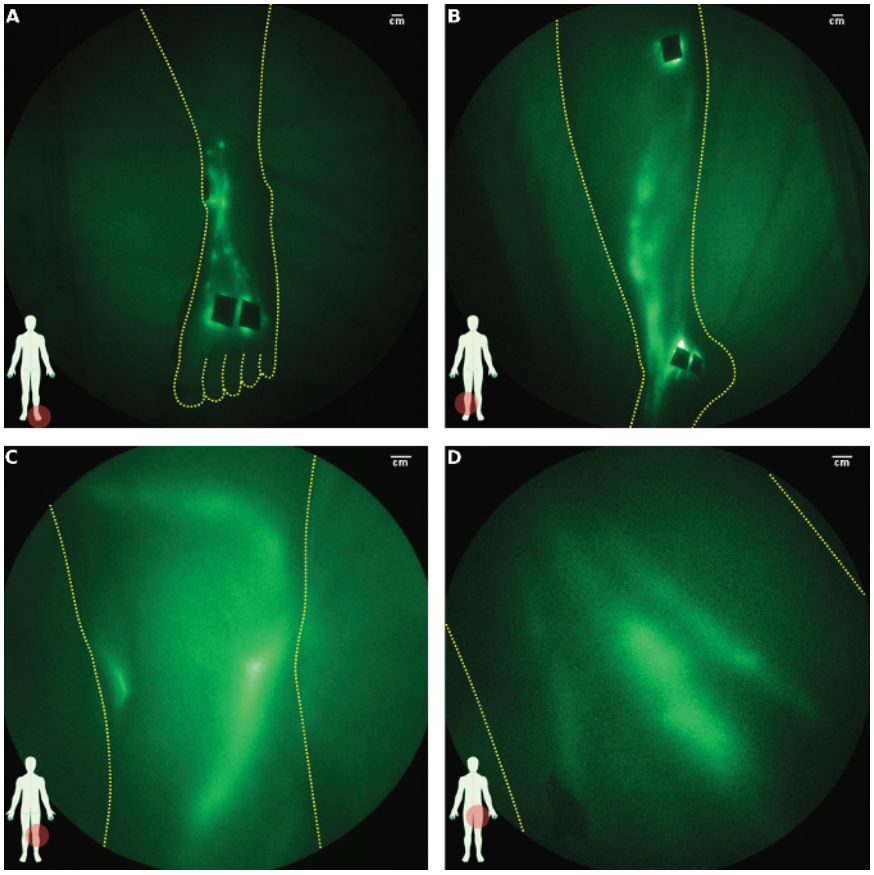

Figure 3. Images of lymphatics of control leg subjects: (A) left foot (subject CL09, Video W2 shows typical lymphatic flow), (B) lower leg (subject CL08), (C) back of knee (subject CL12), and (D) thigh (subject CL03).

shows extravascular fluorescence just above and below the wrist with a conducting lymphatic channel connecting the two areas, whereas the asymptomatic hand has well-defined lymphatic architecture (Figure 4*B*). In Figure 4*C*, the medial view of a symptomatic elbow exhibited extravascular fluorescence and tortuous vessels, but only a single lymphatic vessel was observed on the asymptomatic arm (Figure 4*D*). One subject, who underwent bilateral mastectomies 9 years apart and developed clinically diagnosed unilateral right arm LE approximately 1 year before the second (left breast) mastectomy, is noteworthy. Her right, symptomatic arm had extravascular fluorescence throughout the entire arm (Figure 4*E*), whereas the left, clinically unremarkable asymptomatic arm had two areas of fluorescent lymphatic capillaries with tortuous vessels near the wrist and upper arm (Figure 4*F* [see Figure W1 for magnified images of abnormalities]) as well as backward propagation of fluorescence in the main lymphatic channel just above the wrist. Another noteworthy case is that of a postmastectomy subject who had active backward propulsion of fluorescence into her hand and fingers as evidenced by the bright fluorescent signal emanating from her hand (Figure 4*G*). Incidentally, a spontaneous fistula or "weep hole" had developed in her palm (Figure 4*H*) from which, as reported by the subject, fluid leaked periodically. Interestingly, manual lymphatic drainage therapy did not mitigate her LE.

Figure 5*A* shows a closer view of a lymphatic vessel with apparent backward propagation of fluorescent packets in the asymptomatic limb previously shown in Figure 4*F* (see Video W4 for visualization). Figure 5*B* shows a three-dimensional plot of the fluorescent intensity as a function of time and distance traveled along the lymphatic vessel. By tracking the appearance of the "peaks" of fluorescence, the forward and subsequent retrograde propagation of each fluorescent packet can be identified. Figure 5*C* shows the fluorescent intensity profiles for two ROIs (Figure 5*A*) located 8 cm apart.

While active contractile transport was observed in every asymptomatic arm of persons with LE, only three propulsion events were observed in two asymptomatic arms, whereas two or fewer propulsion events were seen in six symptomatic limbs. As shown in Table 2, the mean ± SD apparent velocities in the symptomatic and asymptomatic arms were 0.7 ± 1.0 and 0.8 ± 0.4 cm/sec, respectively, and the mean ± SD periods were 32.1 ± 17.9 and 39.7 ± 29.1 seconds, respectively. On average, 60 ± 76 more packets were seen in the asymptomatic arms than the contralateral symptomatic limbs. The overall propulsion rates were 1.2 ± 1.0 and 0.3 ± 0.3 propulsions per minute for the asymptomatic and symptomatic arms, respectively, as shown in Table 2. Retrograde propagation of fluorescence was observed in the arms of two subjects with LE.

Asymptomatic and Symptomatic Legs

Many of the lymphatic architectural features seen in symptomatic and asymptomatic arms also occurred in leg LE. As an example, Figure 6*A* indicates extensive extravascular fluorescence over much of the symptomatic leg, whereas the asymptomatic leg appears to have few but well-defined lymphatics vessels. However, a closer examination of the ankles of the same subject (Figure 6*B*; see Figure W2 for magnified images) reveals an abnormal tortuous lymphatic vessel draining from the injection site toward the bottom of the asymptomatic foot,

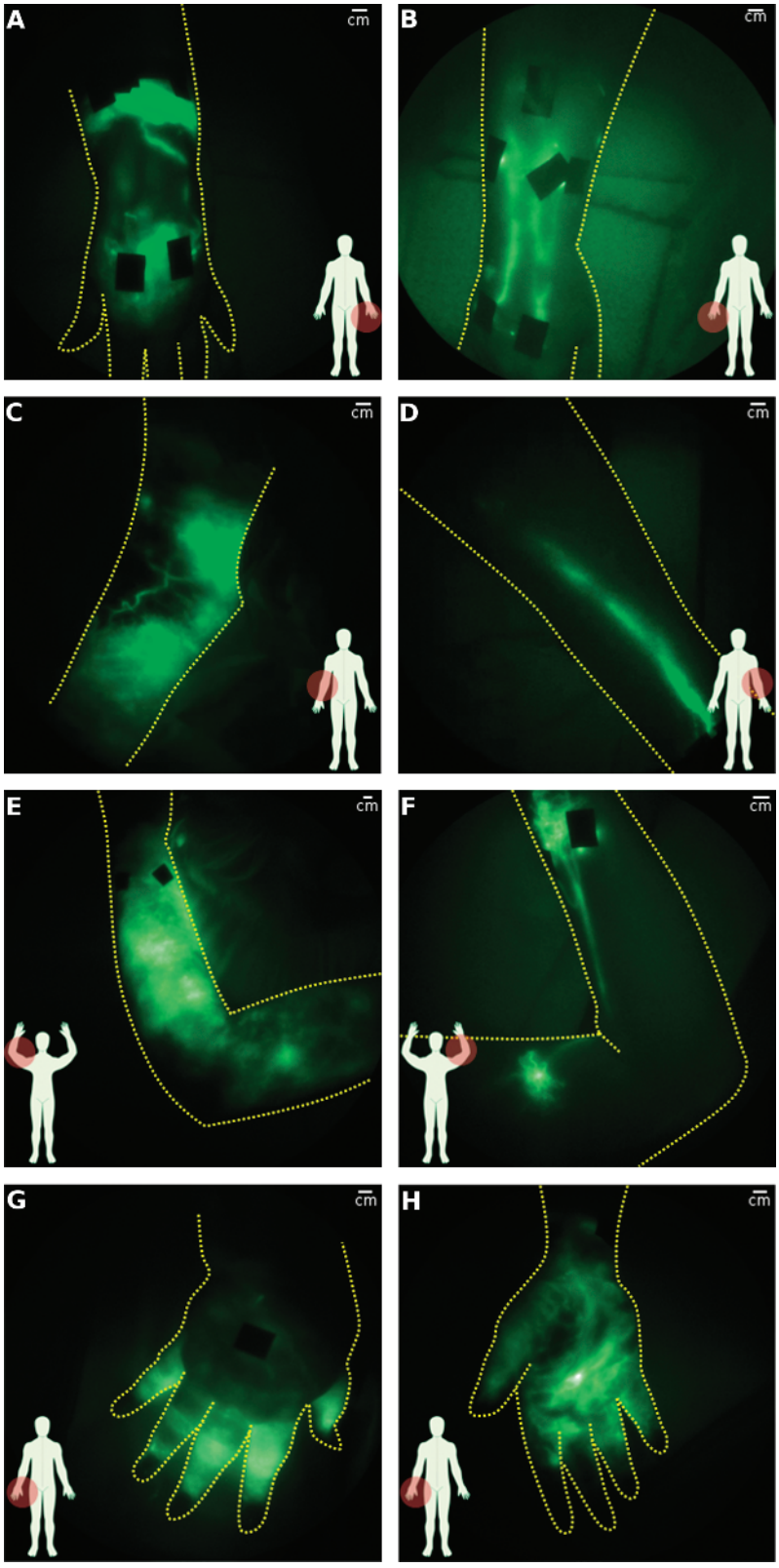

Figure 4. Comparison of lymphatic architecture in symptomatic and asymptomatic arms. (A, C, and E) present images of the symptomatic arm, whereas (B, D, and F) present images of the contralateral asymptomatic arms of three subjects. (A) Symptomatic hand with extravascular fluorescence from injection sites and some networks of fluorescent lymphatic capillaries and (B) normal-looking asymptomatic hand (subject LA06). (C) Symptomatic arm with extravascular fluorescence and tortuous vessels and (D) normal-looking asymptomatic arm (subject LA08). (E) Symptomatic arm with extravascular fluorescence and (F) asymptomatic arm with fluorescent lymphatic capillaries, tortuous lymph vessels, and lymph reflux (subject LA03; Figure 6). (G) Back and (H) front of symptomatic hand in which active lymphatic propulsion was seen pushing fluid into hand (subject LA01). Bright spot on palm (H) is a spontaneous fistula or weep hole that developed to permit lymph to drain.

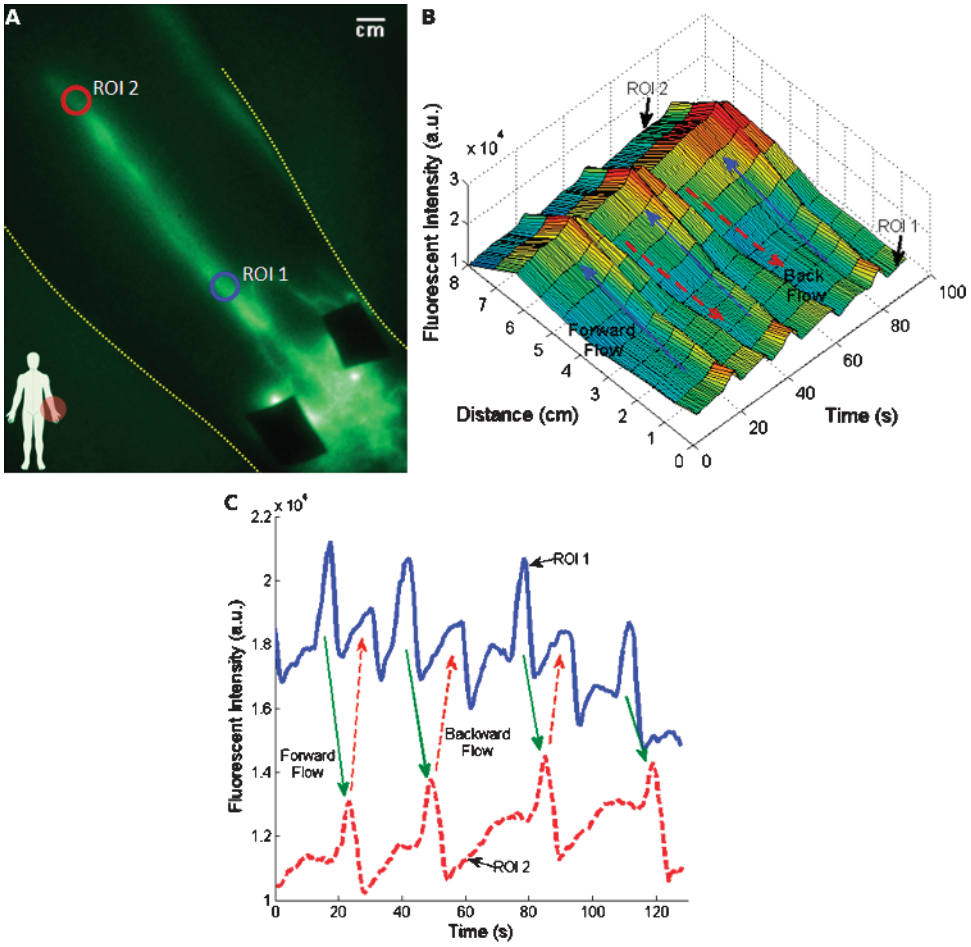

Figure 5. Lymphatic reflux. (A) A closer view of the lymph vessel with lymph reflux in the asymptomatic arm of subject LA03 seen in Figure 4*F* (Video W3 for visualization). In this example, there appears to be insufficient valvular function allowing a portion of each forward moving packet to drain back from ROI 2 (red) to ROI 1 (blue) as illustrated in (B) a three-dimensional plot of fluorescent intensity as a function of time and distance. By following the intensity peaks, the direction of flow is determined. (C) Fluorescent intensity profiles at ROIs 1 and 2.

although no fluorescence is visible in the sole of the asymptomatic foot, whereas extravascular fluorescence is observed in the sole of the symptomatic foot (Figure 6*C*). Figure 6*D* shows both legs of a subject who was clinically diagnosed with unilateral LE of the right leg after right inguinal lymph node dissection. Whereas the asymptomatic leg shows some lymphatic structure, both legs have extensive regions of extravascular fluorescence, which may be indicative of undiagnosed, subclinical lymphedema in the asymptomatic limb. The bright signal outside the limb tracing in Figure 6, *A* and *C*, is due primarily to reflection of the bright fluorescent signal, generated by extravascular ICG, off the imaging bed and secondarily to excitation light leakage.

Of the 10 unilateral leg LE cases investigated, 2 subjects had no observed lymph contractile function in the symptomatic limb. As shown in Table 2, the mean ± SD apparent velocities in the symptomatic and asymptomatic legs were 0.8 ± 0.4 and 0.8 ± 0.5 cm/sec, respectively, and the mean ± SD periods were 72.1 ± 45.1 and 65.3 ± 46.4 seconds, respectively. On average, 6 ± 13 more packets were seen in the asymptomatic legs than in the contralateral symptomatic legs. The overall propulsion rates were 0.3 ± 0.2 and 0.2 ± 0.2 propulsions per minute for the asymptomatic and symptomatic legs, respectively, as shown in Table 2.

Overall Propulsion Rate

Our linear statistical models indicate that diagnosis and limb have a significant effect on the overall propulsion rate with $P < .05$ and $P < .0005$, respectively. As shown in Table 2, the legs consistently have lower mean propulsion rates compared with the arms, whereas both arms and legs have lower mean propulsion rates in the symptomatic limbs. No statistical impact due to side or dose was observed.

Discussion and Conclusions

In this study, we qualitatively and quantitatively compared architectural and contractile functional differences between the lymphatics of control and clinically diagnosed unilateral LE subjects. Both primary and secondary LE are chronic, progressive, and largely uncharacterized diseases that our study sought to capture at one time point for comparison to presumed "normal" control subjects. In addition, the cause of LE, whether genetic or acquired, is in itself controversial because genetic susceptibility for acquiring LE after surgery or trauma remains to be determined. We are unaware whether the observed abnormal patterns of lymphatic architecture and function in LE subjects existed before trauma or before onset of symptoms. Nonetheless, by examining presumed "normal" controls and clinically diagnosed LE subjects, we sought to

image key differences between normal lymphatic architecture and contractile transport function and dysfunction using microgram amounts of fluorescent contrast agent.

Lymphatic Architecture

The architectural characteristics of the lymphatic systems imaged in the LE subjects are striking, not readily amendable for immediate quantitative analysis, and not generally seen in the control subjects, possibly making them excellent diagnostic indicators of lymphatic disorders. Extravascular accumulation of dye especially near the injection sites (for examples, see Figure 4) seen in LE subjects may be attributed to result from failure of initial lymphatic collection (as visualized in $Chy^{+/-}$ animals studies with vascular endothelial growth factor receptor 3 mutation [27]). It remains to be investigated why fluorescent networks of lymphatic capillaries appear in distinct regions often distal to the site of surgical trauma as in the asymptomatic arm of the double mastectomy subject (Figure 4*F*). Architectural features of 1) extravascular dye accumulation and 2) fluorescent capillary networks were only seen in 2 of 48 limbs of control subjects but were observed in all 20 symptomatic and 7 of 20 asymptomatic limbs of LE subjects. Of the seven subjects with these features on the asymptomatic limb, two were diagnosed with primary LE (no known trauma before onset), two developed LE after insect bites, and three (two arms and one leg) developed LE after surgery.

Tortuous vessels are prevalent in both symptomatic and asymptomatic limbs of LE subjects (14/20) and were also visualized in 5 of 24 control subjects. It is unknown whether the presence of tortuous vessels in otherwise normal-looking control subjects is 1) benign with no prognostic indication, 2) indicative of an undiagnosed lymphatic malformation or disorder that could portend complications after lymphatic assault, or 3) as suggested by some of the subject's personal accounts of prior medical history, associated with presumptive lymphangiogenesis related to prior injury or trauma. The role of the lymphatics in tissue repair mechanisms remains unknown.

Lymphatic Contractile Function

In the unilateral arm LE and control subjects studied, our statistical models indicate that there is a significant contribution to the apparent propagation velocities and periods by diagnosis and, in the case of periodicity, limb. However, the high variability of these measurements may preclude classification of disease based on apparent propagation velocity, period, or propulsion rate alone. Figure 7 presents whiskered

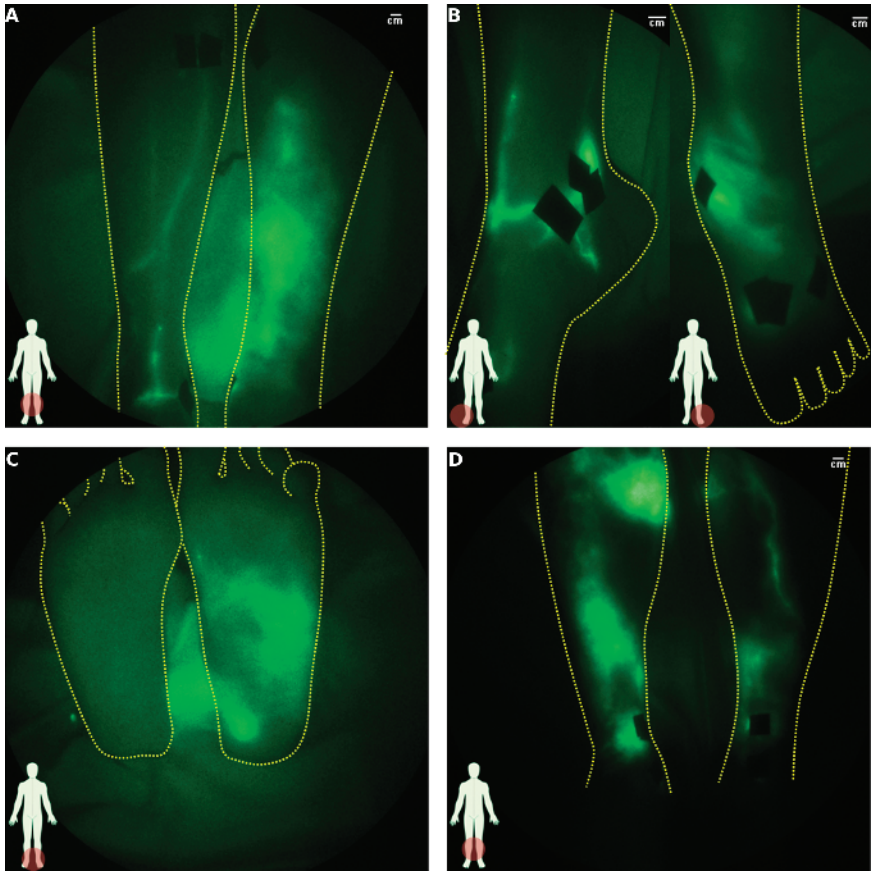

Figure 6. Comparison of architecture in symptomatic and asymptomatic legs. (A) Lower legs of a 23-year-old woman (subject LL05) with lymphedema on the left leg (right in images). Asymptomatic limb looks normal, although it has a paucity of lymphatic vessels, whereas the symptomatic limb has diffuse extravascular fluorescence with no distinct structure. (B) A closer look at the ankles of the same subject as (A) shows that the asymptomatic limb has a tortuous vessel emanating from the injections site, whereas the symptomatic limb shows diffuse extravascular fluorescence again with perhaps a large curved lymphatic vessel just above the ankle bone. (C) Image illustrating the diffusion of dye into the symptomatic foot of the same subject. (D) Lower legs of a 65-year-old woman (subject LL10) with clinically diagnosed lymphedema on the right leg (left in image). Both symptomatic and asymptomatic legs show extensive diffuse extravascular fluorescence, although some structure is apparent in asymptomatic limb.

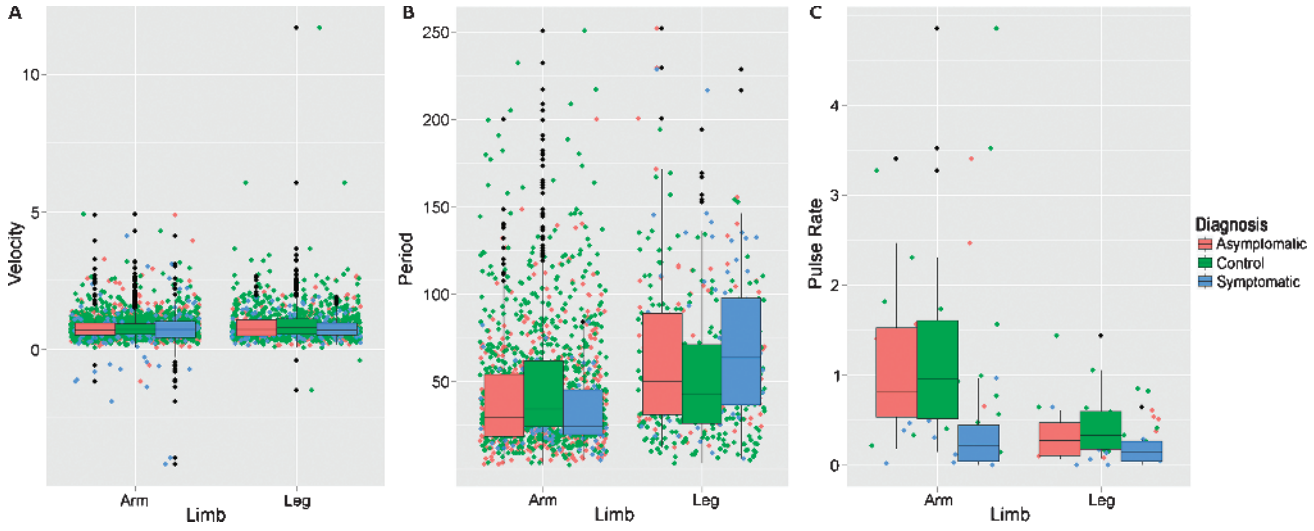

Figure 7. Box plots of (A) apparent propagation velocity, (B) period, and (C) propulsion rate as a function of limb and diagnosis. Also shown is the measurement jitter (colored dots) that illustrates the magnitude of all measurements made and the outliers (black dots).

box plots of the apparent velocity and period measurements as well as the propulsion rate as functions of diagnosis and limb. The colored dots illustrate the actual scatter of the measurements, whereas the black dots indicate the presence of outliers. The lack of classifiable differences seems to indicate that despite the disease status and/or the presence of lymphatic abnormalities in the limb, the apparent propagation velocity and period remain similar. The high variability of these quantities is reflective of the complex and poorly understood physiology that regulates lymphatic function. Perhaps as our understanding of the lymphatics improves, it may be possible to take into account the regulatory physiology with other measurements such as hydration levels or transmural pressure to accomplish diagnostic, quantitative, NIR fluorescence lymphatic imaging.

More propulsion events were consistently observed in control and asymptomatic limbs than symptomatic limbs but again the large variability may prevent its use as a means to classify disease. The lower propulsion rates observed in symptomatic limbs may be due to the tendency to visualize fewer functional lymphatic vessels compared with control and asymptomatic limbs resulting in a net reduction of lymph transport to draining nodal basins as commonly seen in lymphoscintigraphy.

We observed backward propagation of the fluorescent signal in the asymptomatic arm of a breast cancer–related LE subject (LA03; Figures 4*F* and 5 and Video W3) and in the legs of two control subjects (CL04 and CL05) that is a result of lymphatic reflux and could be attributed to lymph valvular insufficiency or to retrograde propagation of lymphatic contractions as has been documented previously in *in situ* studies of rats [28]. Whether the backward propagation or reflux existed in the lymphedema subjects before surgical insult and/or portends the development of LE remains to be evaluated in longitudinal studies of subjects undergoing nodal dissections.

Images of deeper lymphatics, such those seen in the back of the knee (Figure 3*C*), the thigh (Figure 3*D*), and the upper arm (top of Figure 1*C*), often are not as well focused as the lymphatics seen in the hands and feet. This broadening of the structure is due to the scatter the fluorescent signal experiences as it propagates from the lymphatics to the surface of the skin. Scatter and absorption of photons will likely limit the ability to noninvasively image lymphatic structure deeper than several centimeters with our imaging system. However, efforts are underway to develop three-dimensional fluorescence tomography systems that may be able to resolve deeper lymphatics. Whereas penetration depth is an issue with fluorescence imaging because of the physics of light propagation in tissue, this study and that of others (see Marshall et al. [19] for a review of lymphatic imaging with ICG) illustrate the potential of NIR fluorescent imaging to further our understanding of the lymphatics and its spectrum of disease.

In conclusion, in this feasibility study, we have demonstrated the ability to noninvasively interrogate healthy and diseased human lymphatics *in vivo* using microdose injections of ICG and NIR fluorescence imaging. Our ability to see real-time contractile function in health and disease using microgram doses of contrast agent is a result of the increased sensitivity of our instrument compared with other NIR fluorescence imagers found in the literature [19]. The lack of literature on NIR fluorescence imaging of real-time contractile lymphatic function may indicate that 1) existing imaging systems do not have the necessary sensitivity owing to high amounts of excitation light leakage and/or 2) the administration of milligram amounts of ICG may inhibit its visualization by "saturating" the lymphatic vessels with fluorophore, preventing subtle variations in fluorophore concentration or volume from being imaged. The ability to visualize microgram amounts of contrast agents also presents the opportunity to introduce new first-in-human agents under the reduced safety and toxicity requirements of microdosing [29].

Although quantitative functional differences of apparent propagation velocity and period were too subtle to classify individual lymphatic disease in this phase 0 trial, NIR fluorescence provided exquisite information on lymphatic architecture and may provide a much needed tool to enhance our understanding of lymphovascular disease and may potentially aid in diagnosing and phenotyping lymphatic disease for determining cancer patient susceptibility to postsurgical lymphatic complications. Our observations of lymphatic phenotypes in asymptomatic arms and legs may indicate subclinical disease and warrant further investigation. Recent NIR fluorescent imaging data [30] showing initial loss of contractile function and extensive remodeling of lymphatic architecture in association with cancer metastasis in animals suggest the use of NIR fluorescence imaging to 1) not only detect the early stages of cancer

metastasis in humans but also perhaps to 2) provide an early end point, showing inhibition or regression of lymphangiogenesis in response to these emerging antimetastasis therapeutics.

References

[1] Swartz MA (2001). The physiology of the lymphatic system. *Adv Drug Deliv Rev* **50**(1–2), 3–20.

[2] Sakorafas GH, Peros G, Cataliotti L, and Vlastos G (2006). Lymphedema following axillary lymph node dissection for breast cancer. *Surg Oncol* **15**(3), 153–165.

[3] Farncombe M, Daniels G, and Cross L (1994). Lymphedema—the seemingly forgotten complication. *J Pain Symptom Manage* **9**(4), 269–276.

[4] Rockson SG (2001). Lymphedema. *Am J Med* **110**(4), 288–295.

[5] Ridner SH (2006). Pretreatment lymphedema education and identified educational resources in breast cancer patients. *Patient Educ Couns* **61**(1), 72–79.

[6] Mansel RE, Fallowfield L, Kissin M, Goyal A, Newcombe RG, Dixon JM, Yiangou C, Horgan K, Bundred N, Monypenny I, et al. (2006). Randomized multicenter trial of sentinel node biopsy *versus* standard axillary treatment in operable breast cancer: the ALMANAC Trial. *J Natl Cancer Inst* **98**(9), 599–609.

[7] Armer JM (2005). The problem of post–breast cancer lymphedema: impact and measurement issues. *Cancer Invest* **23**(1), 76–83.

[8] de Vries M, Vonkeman WG, van Ginkel RJ, and Hoekstra HJ (2006). Morbidity after inguinal sentinel lymph node biopsy and completion lymph node dissection in patients with cutaneous melanoma. *Eur J Surg Oncol* **32**(7), 785–789.

[9] Finegold DN, Schacht V, Kimak MA, Lawrence EC, Foeldi E, Karlsson JM, Baty CJ, and Ferrell RE (2008). HGF and MET mutations in primary and secondary lymphedema. *Lymphat Res Biol* **6**(2), 65–68.

[10] Karkkainen MJ, Ferrell RE, Lawrence EC, Kimak MA, Levinson KL, McTigue MA, Alitalo K, and Finegold DN (2000). Missense mutations interfere with VEGFR-3 signalling in primary lymphoedema. *Nat Genet* **25**(2), 153–159.

[11] Irrthum A, Devriendt K, Chitayat D, Matthijs G, Glade C, Steijlen PM, Fryns JP, Van Steensel MA, and Vikkula M (2003). Mutations in the transcription factor gene *SOX18* underlie recessive and dominant forms of hypotrichosis-lymphedema-telangiectasia. *Am J Hum Genet* **72**(6), 1470–1478.

[12] Fang J, Dagenais SL, Erickson RP, Arlt MF, Glynn MW, Gorski JL, Seaver LH, and Glover TW (2000). Mutations in FOXC2 (MFH-1), a forkhead family transcription factor, are responsible for the hereditary lymphedema-distichiasis syndrome. *Am J Hum Genet* **67**(6), 1382–1388.

[13] Brice G, Mansour S, Bell R, Collin JR, Child AH, Brady AF, Sarfarazi M, Burnand KG, Jeffery S, Mortimer P, et al. (2002). Analysis of the phenotypic abnormalities in lymphoedema-distichiasis syndrome in 74 patients with FOXC2 mutations or linkage to 16q24. *J Med Genet* **39**(7), 478–483.

[14] Kriederman BM, Myloyde TL, Witte MH, Dagenais SL, Witte CL, Rennels M, Bernas MJ, Lynch MT, Erickson RP, Caulder MS, et al. (2003). FOXC2 haploinsufficient mice are a model for human autosomal dominant lymphedema-distichiasis syndrome. *Hum Mol Genet* **12**(10), 1179–1185.

[15] Kume T, Jiang H, Topczewska JM, and Hogan BL (2001). The murine winged helix transcription factors, Foxc1 and Foxc2, are both required for cardiovascular development and somitogenesis. *Genes Dev* **15**(18), 2470–2482.

[16] Sharma R, Wendt JA, Rasmussen JC, Adams KE, Marshall MV, and Sevick-Muraca EM (2008). New horizons for imaging lymphatic function. *Ann N Y Acad Sci* **1131**, 13–36.

[17] Szuba A and Rockson SG (1998). Lymphedema: classification, diagnosis and therapy. *Vasc Med* **3**(2), 145–156.

[18] Lucarelli RT, Ogawa M, Kosaka N, Turkbey B, Kobayashi H, and Choyke PL (2009). New approaches to lymphatic imaging. *Lymphat Res Biol* **7**(4), 205–214.

[19] Marshall MV, Rasmussen JC, Tan I-C, Aldrich MB, Adams KE, Wang X, Fife CE, Maus EA, Smith LA, and Sevick-Muraca EM (2010). Near-infrared fluorescence imaging in humans with indocyanine green: a review and update. *Open Surg Oncol J* **2**, 12–25.

[20] Rasmussen JC, Tan IC, Marshall MV, Fife CE, and Sevick-Muraca EM (2009). Lymphatic imaging in humans with near-infrared fluorescence. *Curr Opin Biotechnol* **20**(1), 74–82.

[21] Unno N, Nishiyama M, Suzuki M, Yamamoto N, Inuzuka K, Sagara D, Tanaka H, and Konno H (2008). Quantitative lymph imaging for assessment of lymph function using indocyanine green fluorescence lymphography. *Eur J Vasc Endovasc Surg* **36**(2), 230–236.

[22] Unno N, Inuzuka K, Suzuki M, Yamamoto N, Sagara D, Nishiyama M, and Konno H (2007). Preliminary experience with a novel fluorescence lymphography using indocyanine green in patients with secondary lymphedema. *J Vasc Surg* **45**(5), 1016–1021.

[23] Suzuki M, Unno N, Yamamoto N, Nishiyama M, Sagara D, Tanaka H, Mano Y, and Konno H (2009). Impaired lymphatic function recovered after great saphenous vein stripping in patients with varicose vein: venodynamic and lymphodynamic results. *J Vasc Surg* **50**(5), 1085–1091.

[24] Sevick-Muraca EM, Sharma R, Rasmussen JC, Marshall MV, Wendt JA, Pham HQ, Bonefas E, Houston JP, Sampath L, Adams KE, et al. (2008). Imaging of lymph flow in breast cancer patients after microdose administration of a near-infrared fluorophore: feasibility study. *Radiology* **246**(3), 734–741.

[25] Desmettre T, Devoisselle JM, and Mordon S (2000). Fluorescence properties and metabolic features of indocyanine green (ICG) as related to angiography. *Surv Ophthalmol* **45**(1), 15–27.

[26] Team RDC (2008). *R: A Language and Environment for Statistical Computing.* (2.8.1 ed.). R Foundation for Statistical Computing, Vienna, Austria.

[27] Karkkainen MJ, Saaristo A, Jussila L, Karila KA, Lawrence EC, Pajusola K, Bueler H, Eichmann A, Kauppinen R, Kettunen MI, et al. (2001). A model for gene therapy of human hereditary lymphedema. *Proc Natl Acad Sci USA* **98**(22), 12677–12682.

[28] Zawieja DC, Davis KL, Schuster R, Hinds WM, and Granger HJ (1993). Distribution, propagation, and coordination of contractile activity in lymphatics. *Am J Physiol Heart Circ Physiol* **264**(4), H1283–H1291.

[29] Guidance for Industry, Investigators, and Reviewers (2006). *Exploratory IND Studies*. U.S. Department of Health and Human Services, Food and Drug Administration CDER, Rockville, MD.

[30] Kwon S and Sevick-Muraca EM (2010). Functional lymphatic imaging in tumor-bearing mice. *J Immunol Methods* **360**(1-2), 167–172.

Table W1. Summary of Demographics, Dosage, Apparent Contractile Propagation Velocity, and Period in Control Arm Subjects.

Subject ID	Age	Sex	Ethnicity*	Dose ICG (μg)	Side	Apparent Propagation Velocity (mm/s)				Period (sec)			
						No. Velocity Measurements	Range	Median	Mean ± SD	No. Period Measurements	Range	Median	Mean ± SD
CA01	46	F	C	375	Left	23	0.4-2.7	0.7	0.9 ± 0.5	12	9-66	36.5	39.1 ± 19.2
					Right	19	0.3-1.0	0.8	0.7 ± 0.2	14	15-65	20.0	24.3 ± 12.3
CA02	59	M	C	375	Left	18	0.3-2.6	0.7	0.9 ± 0.6	9	12.6-62.9	17.8	23.6 ± 16.0
					Right	42	0.3-2.6	0.7	0.8 ± 0.5	23	11.0-39.7	23.9	23.1 ± 8.9
CA03	22	M	C	200	Left	135	0.3-2.6	0.9	0.9 ± 0.3	57	3.4-117.1	42.2	48.6 ± 27.9
					Right	105	0.4-4.9	0.9	1.0 ± 0.6	31	9.5-81.4	30.3	33.8 ± 19.7
CA04	41	F	C	200	Left	36	0.4-2.5	1.0	1.2 ± 0.5	11	15.0-82.6	56.4	48.6 ± 23.7
					Right	87	0.3-3.1	0.8	0.9 ± 0.4	32	8.9-138.2	25.7	41.0 ± 35.1
CA05	46	F	C	200	Left	32	0.4-2.1	0.8	0.9 ± 0.4	13	3.5-199.6	47.0	60.0 ± 53.4
					Right	46	0.4-1.8	0.8	0.9 ± 0.3	11	10.5-43.1	29.1	29.2 ± 11.2
CA06	50	F	AA	200	Left†	47	0.4-1.3	0.8	0.8 ± 0.2	34	18.5-157.7	28.6	32.9 ± 23.2
					Right	105	0.3-1.1	0.8	0.8 ± 0.2	75	7.7-106.1	22.8	27.1 ± 15.4
CA07	36	F	C	200	Left	112	0.2-4.3	0.9	0.9 ± 0.5	53	2.3-85.0	29.5	32.5 ± 18.7
					Right	36	0.3-2.3	0.8	0.9 ± 0.4	18	12.5-116.7	74.6	67.1 ± 36.4
CA08	48	F	C	200	Left	37	0.3-1.6	0.7	0.8 ± 0.3	10	7.7-133.0	42.2	56.8 ± 45.7
					Right	75	0.4-1.7	0.8	0.8 ± 0.2	42	9.3-173.4	40.1	47.8 ± 35.8
CA09	35	F	AA	200	Left	12	0.2-0.7	0.4	0.4 ± 0.2	3	41.0-54.8	45.2	47.0 ± 7.1
					Right	15	0.2-0.8	0.5	0.5 ± 0.1	6	30.5-57.4	39.8	42.5 ± 11.8
CA10	41	F	H	300	Left	61	0.2-2.4	0.7	0.8 ± 0.4	33	13.1-77.9	30.3	33.3 ± 13.4
					Right	48	0.1-1.5	0.9	0.8 ± 0.3	28	15.8-71.5	26.4	31.7 ± 13.4
CA11	35	F	C	300	Left	21	0.3-1.1	0.5	0.6 ± 0.2	15	27.0-208.9	55.4	64.9 ± 47.0
					Right	131	0.2-1.0	0.6	0.6 ± 0.1	107	16.1-188.7	36.7	46.5 ± 28.2
CA12	37	M	A	300	Left	75	0.4-1.0	0.6	0.6 ± 0.1	51	7.0-205.1	71.3	78.1 ± 48.9
					Right	175	0.1-1.2	0.5	0.6 ± 0.2	115	9.0-250.5	77.7	82.0 ± 46.6

*A indicates Asian; AA, African American; C, Caucasian; and H, Hispanic.
†Observed tortuous vessel (T).

Table W2. Summary of Demographics, Dosage, Apparent Contractile Propagation Velocity, and Period in Control Leg Subjects.

Subject ID	Age	Sex	Ethnicity*	Dose ICG (μg)	Side†	Features‡	Apparent Propagation Velocity (cm/sec)				Period (sec)			
							No. Velocity Measurements	Range	Median	Mean ± SD	No. Period Measurements	Range	Median	Mean ± SD
CL01	46	F	C	400	Left	T	44	0.3-2.7	0.8	1.0 ± 0.6	20	15-93	30.5	38.1 ± 21.9
					Right	—	36	0.3-1.6	0.9	0.9 ± 0.3	22	7-167	69.0	69.5 ± 38.2
CL02	23	M	C	262.5	Left	—	27	0.6-6.1	1.9	2.2 ± 1.4	16	7.6-153.9	13.8	40.5 ± 47.6
					Right	—	8	0.8-1.8	1.3	1.3 ± 0.4	0	—	—	—
CL03	29	F	C	400	Left	—	45	0.3-1.4	0.6	0.7 ± 0.3	10	31.4-118.2	45.6	63.6 ± 33.1
					Right	—	42	0.3-1.9	0.7	0.8 ± 0.4	15	14.2-95.1	46.3	49.1 ± 24.7
CL04	27	F	C	350	Left	—	68	0.4-3.2	0.9	1.1 ± 0.6	16	9.6-169.0	63.1	70.3 ± 40.1
					Left, Back	R	1	−1.5	−1.5	—	0	—	—	—
					Right	—	15	0.3-1.6	0.8	0.8 ± 0.4	1	78.3	78.3	—
CL05	29	F	C	375	Left	—	29	0.5-2.0	0.8	0.9 ± 0.4	6	41.2-110.6	57.9	65.1 ± 27.7
					Left, Back	R	1	−0.4	−0.4	—	0	—	—	—
					Right	T	23	0.5-1.4	0.7	0.8 ± 0.3	5	15.5-97.5	57.5	52.0 ± 31.2
CL06	35	F	C	400	Left	—	5	0.8-1.2	0.9	1.0-0.2	0	—	—	—
					Right	—	19	0.3-2.1	0.8	1.0 ± 0.5	7	15.9-85.3	28.5	39.7 ± 25.1
CL07	52	F	C	350	Left	T	53	0.2-2.4	0.7	0.8 ± 0.4	17	10.3-96.6	20.9	33.4 ± 28.6
					Right	EF	45	0.2-1.2	0.6	0.6 ± 0.3	22	10.1-132.3	35.9	40.4 ± 27.7
CL08	40	F	A	400	Left	—	35	0.2-2.3	0.6	0.7 ± 0.4	15	6.9-125.0	33.2	35.1 ± 27.9
					Right	—	45	0.3-1.9	0.6	0.8 ± 0.4	29	13.8-110.2	33.9	42.1 ± 24.0
CL09	25	F	C	400	Left	—	42	0.2-2.5	0.8	1.1 ± 0.7	21	3.2-193.8	82.4	78.1 ± 54.6
					Right	—	3	0.3-1.1	0.7	0.7 ± 0.4	0	—	—	—
CL10	34	F	C	400	Left	—	20	0.4-1.4	0.9	0.9 ± 0.2	12	12.3-125.4	78.4	77.0 ± 37.5
					Right	—	17	0.3-1.8	0.8	0.9 ± 0.5	5	32.5-110.3	51.3	64.3 ± 34.9
CL11	22	M	C	400	Left	T, H	30	0.1-1.7	0.8	0.7 ± 0.4	10	27.6-107.4	58.0	58.5 ± 23.5
					Right	—	12	0.4-1.3	1.0	0.9 ± 0.3	3	50.0-107.0	55.4	70.8 ± 31.5
CL12	59	F	C	400	Left	—	36	0.4-2.7	0.9	1.0 ± 0.5	12	28.3-83.3	40.5	44.3 ± 15.4
					Right	—	33	0.1-11.7	1.0	1.4 ± 2.0	9	4.8-152.6	31.9	43.9 ± 46.5

*A indicates Asian; AA, African American; C, Caucasian; and H, Hispanic.
†Back = Backward movement.
‡Features noted include tortuous vessels (T), hyperplastic lymphatic networks (H), extravascular fluorescence (EF), and reflux or retrograde propagation (R).

Table W3. Summary of Demographics, Dosage, Disease Cause, Apparent Contractile Propagation Velocity, and Period in Subjects with Unilateral Arm Lymphedema.

Subject ID	Age	Sex	Ethnicity*	Dose ICG (μg)	Cause and Comments	Diagnosis, Side†	Features‡	Apparent Propagation Velocity (cm/sec)				Period (sec)			
								No. Velocity Measurements	Range	Median	Mean ± SD	No. Period Measurements	Range	Median	Mean ± SD
LA01	46	F	C	400	Onset after mastectomy.	Symp, L	EF	0	—	—	0	0	—	—	—
					Had spontaneous fistula	Symp, L, Back	ABP	12	−4.2 to −0.5	−1.0	−1.5 ± 1.3	9	15.9-24.3	20.9	20.7 ± 2.7
					for lymph drainage in	Asym, R	—	5	0.2 to 1.0	0.5	0.5 ± 0.3	0	—	—	—
					palm of symptomatic hand.										
LA02	66	F	C	300	Onset after mastectomy.	Asym, L	EF	50	0.5 to 3.3	0.9	1.0 ± 0.5	27	3.5-78.8	31.5	38.5 ± 23.4
						Symp, R	EF, H, T	2	0.2	0.2	0.2	1	56.9	56.9	56.9
LA03	62	F	C	300	Onset after mastectomy (right),	Asym, L	H, R	10	0.5 to 1.6	0.9	0.9 ± 0.4	7	11.3-117.0	37.6	48.0 ± 41.5
					had second mastectomy (left)	Asym, L, Back	H, R	2	−1.2 to −0.6	−0.9	−0.9 ± 0.4	1	67.4	67.4	67.4
					9 years after the first. Edema	Symp, R	EF, H	10	0.4 to 4.1	1.6	1.8 ± 1.0	9	8.4-54.6	12.0	19.2 ± 14.5
					commenced ~1 year before										
					the second mastectomy.										
LA04	48	F	C	312.5	Onset after melanoma surgery.	Symp, L	EF	13	0.6 to 2.2	1.1	1.1 ± 0.4	8	11.0-82.5	44.5	43.6 ± 20.0
					Bilateral lymphedema on legs.	Asym, R	—	19	0.5 to 1.3	0.8	0.8 ± 0.2	6	6.4-15.3	10.7	10.9 ± 3.4
LA05	56	F	H	325	Onset after mastectomy.	Asym, L	—	57	0.2 to 1.2	0.5	0.6 ± 0.3	33	16.5-117.3	38.1	45.4 ± 28.4
						Symp, R	H, T	14	0.2 to 1.4	0.4	0.4 ± 0.3	11	18.7-24.5	22.2	22.1 ± 1.7
LA06	68	F	C	300	Onset after mastectomy.	Symp, L	EF, H, T	18	0.4 to 3.1	0.8	1.0 ± 0.8	10	14.5-75.0	32.5	37.1 ± 20.5
						Asym, R	—	38	0.3 to 1.6	0.6	0.6 ± 0.3	14	11.9-140.0	35.1	44.6 ± 34.3
LA07	67	F	C	300	Onset after lumpectomy	Symp, L	EF, H,	1	0.8	0.8	0.8	0	—	—	—
					and axillary dissection.	Asym, R	—	192	0.1 to 4.9	0.9	0.9 ± 0.5	99	2.8-200.0	27.8	33.3 ± 27.4
LA08	81	F	C	250	Onset after mastectomy.	Asym, L	—	49	0.2 to 1.2	0.6	0.6 ± 0.2	24	22.3-111.0	49.8	53.6 ± 23.7
						Symp, R	H, T	10	0.7 to 1.2	0.9	0.9 ± 0.2	9	16.1-24.7	23.5	21.9 ± 3.3
LA09	57	F	C	300	Onset after mastectomy.	Asym, L	—	54	0.4 to 2.9	0.8	0.9 ± 0.4	19	5.7-139.4	56.9	58.1 ± 39.6
						Symp, R	EF, H, T	12	0.1 to 1.7	0.5	0.6 ± 0.5	1	25.0	25.0	25.0
						Symp, R, Back	EF, H, T	1	−0.3	−0.3	−0.3	0	—	—	—
LA10	49	F	C	300	Onset after mastectomy	Symp, L	EF, H, T	45	0.5 to 2.0	0.8	0.8 ± 0.3	39	5.0-84.0	36.1	38.7 ± 19.2
						Asym, R		255	0.1 to 2.5	0.6	0.7 ± 0.3	172	2.8-148.4	27.7	38.5 ± 28.1

*A indicates Asian; AA, African American; C, Caucasian; and H, Hispanic.

†Asym indicates asymptomatic; Symp, symptomatic; L, left; R, right; and Back, backward movement.

‡Features noted include tortuous vessels (T), hyperplastic lymphatic networks (H), extravascular fluorescence (EF), reflux or retrograde propagation (R), and active backward propulsion (ABR).

Table W4. Summary of Demographics, Dosage, Disease Cause, Apparent Contractile Propagation Velocity, and Period in Subjects with Unilateral Leg Lymphedema.

Subject ID	Age	Sex	Ethnicity*	Dose ICG (μg)	Cause and Comments	Diagnosis, Side†	Features‡	Apparent Propagation Velocity (cm/sec)				Period (sec)			
								No. Velocity Measurements	Range	Median	Mean ± SD	No. Period Measurements	Range	Median	Mean ± SD
LL01	18	F	C	400	Onset at age 18 with unknown cause (no record of trauma or surgical procedure).	Symp, L	EF	0	—	—	0	0	—	—	—
						Asym, R	—	3	0.6-1.5	1.0	1.0 ± 0.4	0	—	—	—
LL02	66	F	C	400	Onset after cancer surgery.	Symp, L	H, T	11	0.2-0.8	0.6	0.6 ± 0.2	6	43.8-113.0	60.6	65.9 ± 25.0
						Asym, R	—	15	0.6-1.3	1.0	1.0 ± 0.2	7	25.6-200.5	45.9	77.7 ± 70.3
LL03	36	F	C	400	Onset after trauma (foot sprain).	Symp, L	H, T, EF	14	0.5-0.8	0.7	0.7 ± 0.1	10	24.4-135.3	64.0	62.0 ± 43.1
						Asym, R	—	35	0.3-1.5	0.7	0.7 ± 0.3	24	20.7-117.4	48.1	49.9 ± 26.8
LL04	20	F	C	400	Onset after multiple leg injuries.	Symp, L	H, T, EF	62	0.3-1.9	0.8	0.9 ± 0.4	32	18.6-216.4	58.3	74.5 ± 46.3
						Asym, R	—	49	0.2-2.7	1.0	1.1 ± 0.6	19	13.2-133.2	40.2	55.1 ± 37.2
LL05	23	F	AA	400	Onset occurred after insect bite.	Symp, L	EF	0	—	—	—	0	—	—	—
						Asym, R	T, H	6	0.2-1.1	0.4	0.5 ± 0.3	2	41.7-42.5	42.1	42.1 ± 0.6
LL06	48	F	AA	350	Unknown cause, possibly due to pressure from large, untreated fibroid cyst in uterine system.	Symp, L	EF, H, T	2	0.5-0.5	0.5	0.5 ± 0.0	1	60.4	60.4	60.4
						Asym, R	H, T	3	0.6-1.6	0.7	1.0 ± 0.6	0	—	—	—
LL07	40	F	AA	400	Onset after spider bite on toe, also had fibroid cysts in groin.	Asym, L	T	20	0.1-0.8	0.5	0.5 ± 0.2	8	12.4-229.5	36.9	71.8 ± 74.8
						Symp, R	H, T, EF	15	0.1-1.4	0.7	0.7 ± 0.4	6	6.0-228.3	62.9	83.6 ± 89.7
LL08	31	M	C	400	Onset at age 10 with unknown cause.	Symp, L	H, T	11	0.4-1.9	1.3	1.2 ± 0.5	7	18.6-102.3	83.9	75.5 ± 27.8
						Asym, R	T	12	0.5-1.0	0.6	0.7 ± 0.2	6	31.2-109.5	47.4	62.6 ± 35.8
LL09	47	F	C	50	Onset after cancer surgery. Subject declined additional injections.	Symp, L	EF, H	7	0.3-0.8	0.5	0.5 ± 0.2	6	27.5-141.0	65.8	71.1 ± 39.7
						Asym, R	—	6	0.2-0.8	0.3	0.4 ± 0.2	0	—	—	—
LL10	65	F	A	400	Onset after cancer surgery.	Asym, L	H, T	45	0.1-2.3	0.7	0.8 ± 0.5	25	31.3-252.0	77.7	84.8 ± 48.9
						Symp, R	H, T	11	0.2-0.9	0.4	0.5 ± 0.2	4	28.3-146.3	50.4	68.8 ± 54.2

*A indicates Asian; AA, African American; C, Caucasian; and H, Hispanic.

†Asym indicates asymptomatic; Symp, symptomatic; L, left; R, right; and Back, backward movement.

‡Features noted include tortuous vessels (T), hyperplastic lymphatic networks (H), extravascular fluorescence (EF), and reflux or retrograde propagation (R).

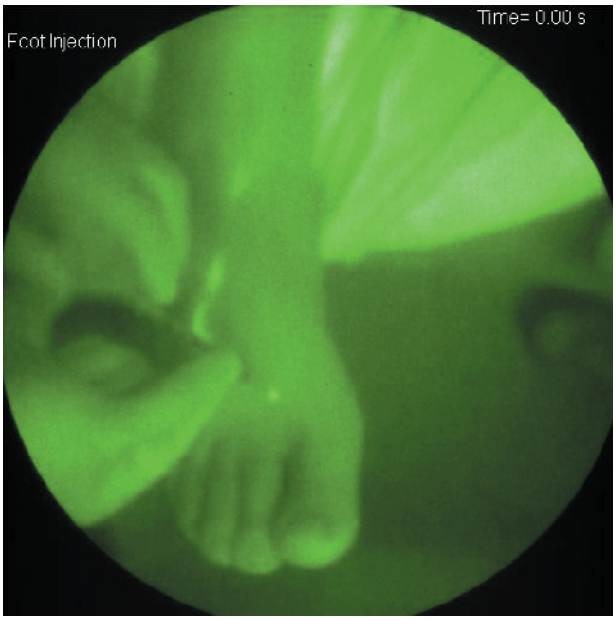

Video W1. Movie of the injection, uptake, and subsequent propulsion of ICG from the injection sites in the foot toward the draining lymph nodes. This movie, although not of high quality because of the movement of the foot, illustrates the similarity of the dye front propagation immediately after ICG administration and the propagation of the fluorescent packets within the lymphatics as observed in Videos W2 and W3.

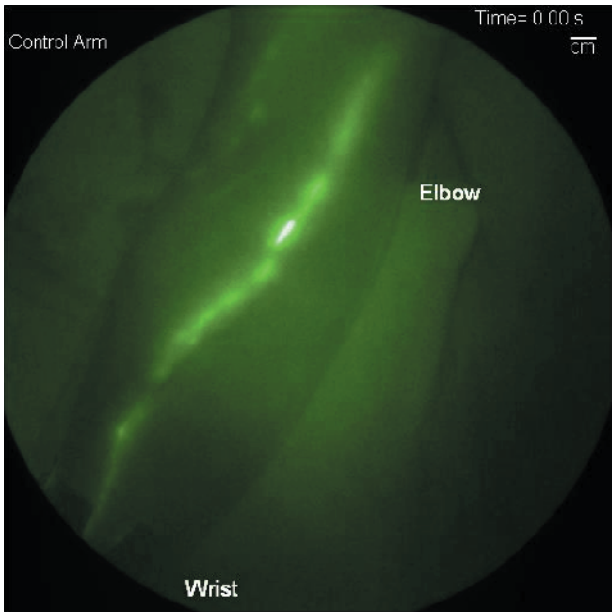

Video W2. Movie of active lymphatic propulsion in the right arm of control subject CA10. Movie is approximately three times faster than real time. Black square is covered injection site.

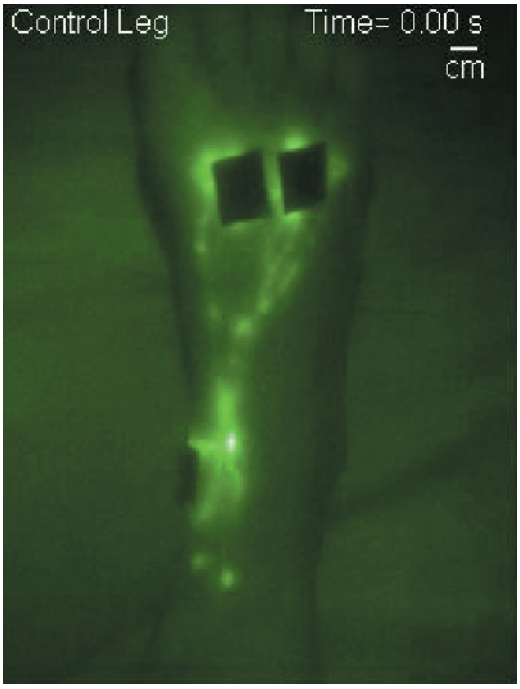

Video W3. Movie of active lymphatic propulsion from injection sites in right foot of control subject CL09. Movie is approximately three times faster than real time. Black squares are covered injection sites.

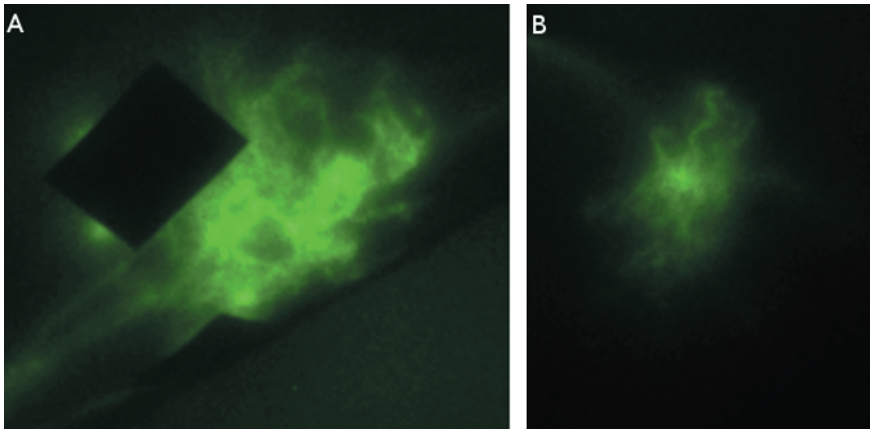

Figure W1. Magnified fluorescent images of the lymphatic malformations seen in the asymptomatic arm of subject LA03 illustrating the dense fluorescent capillary networks and tortuous vessels near the (A) injection sites in the wrist and (B) in the upper arm distal to all injection sites.

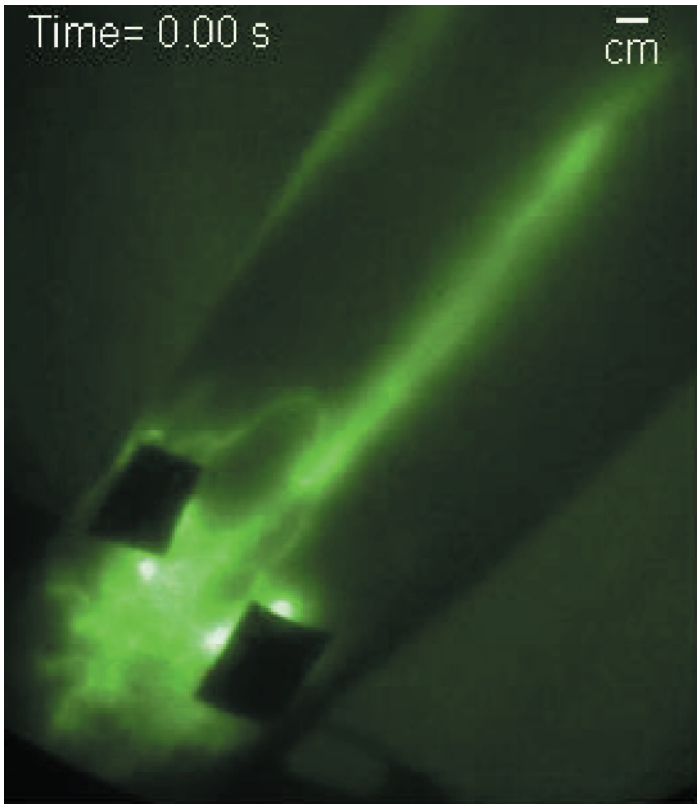

Video W4. Movie of lymphatic reflux in asymptomatic arm of subject LA03. Note the backward movement of fluorescence after each forward propulsion event. Movie is approximately three times faster than real time. Black squares are covered injection sites.

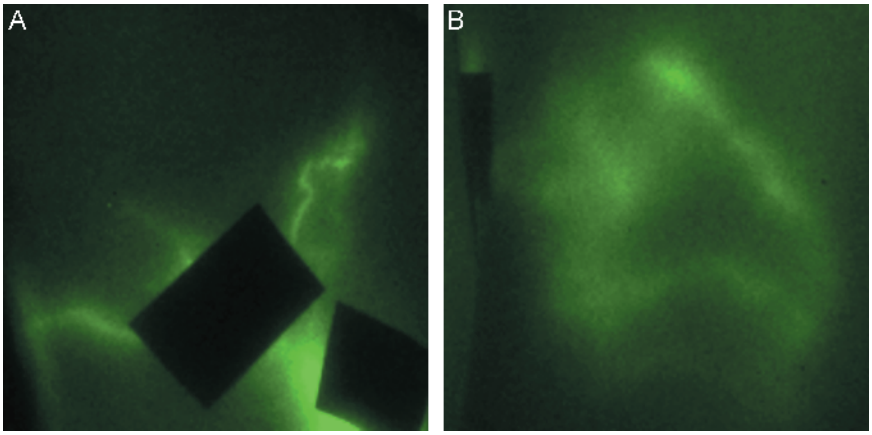

Figure W2. Magnified fluorescent images of the tortuous lymphatic vessels seen in the asymptomatic ankle (subject LL05) on both the (A) medial and (B) lateral sides.